

PREPRINT OMAE2019-95378

IDENTIFYING HIGHER-ORDER INTERACTIONS IN WAVE TIME-SERIES

Kevin Ewans

MetOcean Research Ltd
New Plymouth, New Zealand

Suzana Ilic

Lancaster University, UK

Marios Christou

Imperial College
London, UK

Philip Jonathan

Shell Research Ltd, UK
Lancaster University, UK

ABSTRACT

Reliable design and reanalysis of coastal and offshore structures requires, amongst other things, characterisation of extreme crest elevation corresponding to long return periods, and of the evolution of a wave in space and time conditional on an extreme crest.

Extreme crests typically correspond to focussed wave events enhanced by wave-wave interactions of different orders. Higher-order spectral analysis can be used to identify wave-wave interactions in time-series of water surface elevation.

The bispectrum and its normalised form (the bicoherence) have been reported by numerous authors as a means to characterise three-wave interactions in laboratory, field and simulation experiments. The bispectrum corresponds to a frequency-domain representation of the third order cumulant of the time-series, and can be thought of as an extension of the power spectrum (itself the frequency-domain representation of the second order cumulant). The power spectrum and bispectrum can both be expressed in terms of the Fourier transforms of the original time-series. The Fast Fourier transform (FFT) therefore provides an efficient means of estimation. However, there are a number of important practical considerations to ensuring reasonable estimation.

To detect four-wave interactions, we need to consider the trispectrum and its normalised form (the tricoherence). The trispectrum corresponds to a frequency-domain (Fourier) representation of the fourth-order cumulant of the time-series. Four-wave interactions between Fourier components can involve interactions of the type where $f_1 + f_2 + f_3 = f_4$ and where $f_1 + f_2 = f_3 + f_4$, resulting in two definitions of the trispectrum, depending on which of the two interactions is of interest. We consider both definitions in this paper. Both definitions can be estimated using the FFT, but its estimation is considerably more

challenging than estimation of the bispectrum. Again, there are important practicalities to bear in mind.

In this work, we consider the key practical steps required to correctly estimate the trispectrum and tricoherence. We demonstrate the usefulness of the trispectrum and tricoherence for identifying wave-wave interactions in synthetic (based on combinations of sinusoids and on the HOS model) and measured wave time-series.

INTRODUCTION

The power spectrum, based on Fourier analysis, has been widely used as a tool to study ocean wind waves by scientists and engineers alike, since its introduction for this purpose around 1950. Barber and Ursell (1948) published the first wave spectra, and Pierson and Marks (1952) introduced power spectrum analysis to ocean wave data analysis, following techniques pioneered by Tukey (1949). The wave power spectrum provides a frequency representation of the surface elevation that can be used to identify the most energetic Fourier components for engineering applications, and it is fundamental in numerical wave prediction models.

The power spectrum provides a complete description of the frequency content of the sea surface, if it consists of a linear superposition of statistically independent free waves. However, insight into higher order effects, such as those resulting from three and four wave interactions, require more sophisticated analyses techniques – *viz.* higher-order spectral analysis.

Higher-order spectral analysis is formulated in a general way from the definition of cumulants (Brillinger, 1965). Accordingly, the power spectrum is the Fourier transform of the second-order cumulant, the bispectrum is the Fourier transform of the third-order cumulant, the trispectrum is the Fourier transform of the fourth-order cumulants, and in general, the k^{th} -

order polyspectrum is the Fourier transform of the $(k+1)^{\text{th}}$ -order cumulant.

The bispectrum is a function of two frequencies and provides an estimate of the degree of coupling between wave components at the two frequencies and a third; it is therefore an appropriate tool to investigate triad interactions in a sea state. Hasselman *et al.* (1963) was the first to use the bispectrum to examine such 2nd order interactions in sea states; other examples include Elgar and Guza (1985), Cherneva and Guedes Soares (2007), and Toffoli *et al.* (2007).

The trispectrum is a function of three frequencies and provides an estimate of the degree of coupling between wave components at the three frequencies and a fourth, thus being appropriate for investigating quadruplet interactions in a sea states. Examples of the use of the trispectrum to investigate quadruplet interactions in sea states include Chandran *et al.* (1994), Elgar *et al.* (1995), and Aubourg *et al.* (2017)

Four-wave interactions between Fourier components can involve interactions of the type where $f_1 + f_2 + f_3 = f_4$ and where $f_1 + f_2 = f_3 + f_4$, resulting in two definitions of the trispectrum, depending on which of the two interactions is of interest. The first, appropriate for interactions of the type $f_1 + f_2 + f_3 = f_4$, in a time series, $x(t)$, is given by

$$T(f_1, f_2, f_3) = X(f_1)X(f_2)X(f_3)X^*(f_4)$$

where $f_4 = f_1 + f_2 + f_3$, and for example, $X(f)$ is the Fourier transform of $x(t)$, $X^*(f)$ is the complex conjugate of $X(f)$.

The second, appropriate for interactions of the type $f_1 + f_2 = f_3 + f_4$, is given by

$$V(f_1, f_2, f_3) = X(f_1)X(f_2)X^*(f_3)X^*(f_4)$$

where $f_4 = f_1 + f_2 - f_3$.

It is useful to normalise the higher-order spectra, to enable the degree of nonlinear interaction to be quantified. Several normalisation definitions can be found in the literature. Chandran *et al.* (1994) defines two, both extensions of normalisations of bispectra - one based on that used by Haubrich (1965), and one based on that used by Kim and Powers (1979). Aubourg *et al.* (2017) used a normalisation based on power spectra. The squared magnitude of the bispectrum and trispectrum are often referred to as bicoherence and tricoherence respectively. Thus, for example, the tricoherence, for interactions of the type $f_1 + f_2 + f_3 = f_4$, based on the Kim and Powers (1979) normalisation is defined as

$$t^2(f_1, f_2, f_3) = |\mathcal{T}(f_1, f_2, f_3)|^2$$

where

$$\mathcal{T}(f_1, f_2, f_3) = \frac{E[T(f_1, f_2, f_3)]}{\sqrt{E[|X(f_1)X(f_2)X(f_3)|^2]E[|X(f_4)|^2]}}$$

where $E[\cdot]$ is the expectation operator.

It can be shown that $0 \leq t^2 \leq 1$ (Chandran *et al.*, 1994), which permits the interpretation that the tricoherence is a measure of

the fraction of the total product of powers at the frequency quartet, (f_1, f_2, f_3, f_4) , that are phase-coupled.

In terms of the second trispectrum definition, for interactions of the type $f_1 + f_2 = f_3 + f_4$

$$v^2(f_1, f_2, f_3) = |\mathcal{V}(f_1, f_2, f_3)|^2$$

where

$$\mathcal{V}(f_1, f_2, f_3) = \frac{E[V(f_1, f_2, f_3)]}{\sqrt{E[|X(f_1)X(f_2)X(f_3)|^2]E[|X(f_4)|^2]}}$$

Hinich and Wolinsky (2005) favour a statistical definition for the normalisation and argue that the normalisation based on Kim and Powers (1979) can give misleading results for large sample sizes for which high spectral resolution is possible and used. Nevertheless, the Kim and Powers (1979) definition provides for a convenient interpretation, and records of ocean waves are typically not long enough to allow sufficient reliability in Fourier estimates at very high frequency resolution.

In this paper we compute the t^2 and v^2 tricoherence, which we refer to as T- and V-tricoherence estimates for a number of signals. We begin with various combinations of sine waves, to gather evidence on how the tricoherence estimators might be interpreted in terms of four wave interactions. This experience is then used to evaluate the tricoherence estimates for numerical simulations using a nonlinear wave model, laboratory measurements of a steep sea state that would be expected to involve higher-order wave-wave interactions, and the field measurement recording that includes the famous Draupner wave that is believed to result from higher-order effects. The immediately following section provides a brief description of the spectral estimation technique.

SPECTRAL ESTIMATION METHOD

Spectral analysis of the digital time series signals, $x(t_i)$, are processed following the Welch (1967) method. That is, $x(t_i)$ is divided into L segments, each of length N , a power of 2. $X(f_i)$ for each segment are estimated using the FFT algorithm. The required quantities – e.g. $X(f_i)X(f_j)X(f_k)$, for $X(f_1)X(f_2)X(f_3)$ and $X(f_i)X(f_j)X(f_k)X^*(f_l)$ for $X(f_1)X(f_2)X(f_3)X^*(f_4)$ – are estimated for each segment and the expected values estimated from the average of each quantity over all L segments.

Each segment is windowed with a Hanning window (e.g. Harris, 1978), and may be half-overlapped with adjacent segments, to improve the spectral reliability, or not, if it isn't appropriate for the signal or spectral resolution is not an issue. Accordingly, we have half-overlapped segments in the case of the simulated HOS data and the measured data, to maximise reliability, but we have not overlapped the segments in the case of the sine waves for which reliability is not an issue.

To mitigate spurious large estimates of tricoherence corresponding to occurrences of near-zero values of the denominator in the tricoherence expression, a regularisation parameter of size 0.01 times the numerator is added to the

denominator throughout. This introduces a bias of 1% at the peak tricoherence.

TRICOHERENCE OF SINUSOIDS

Insight into the behaviour of the trispectrum is obtained by examining the trispectrum of a signal $y(t)$ consisting of four sinusoids immersed in a background of Gaussian noise. A theoretical outline for the observed results is given in the Appendix.

$$y_1(t) = \sum_{i=1}^5 a_i \sin(2\pi f_i t + \phi_i)$$

$$y_2(t) = N(0, \text{var}(y_1(t)))$$

$$y(t) = y_1(t) + y_2(t)$$

Where $a_1 = a_2 = a_3 = 1$; $f_1 = 0.0521$ Hz, $f_2 = 0.1437$ Hz, $f_3 = 0.0710$ Hz; $\phi_1 = 0$, $\phi_2 = \pi/16$, $\phi_3 = \pi/3$.

We vary the frequency and phase of the fourth and fifth sinusoids, a_4 , f_4 , ϕ_4 , a_5 , f_5 , and ϕ_5 , for a number of test case as tabulated in Table 1, but in each case $f_5 = f_4$. $U(0, 2\pi)$ in Table 1, denotes the uniform distribution on the interval $[0, 2\pi)$.

Table 1 Fourth and Fifth sinusoid parameters for the five test cases

Case	a_4	f_4	ϕ_4	a_5	ϕ_5
SIN1	1	$f_1 + f_2 + f_3$	$\phi_1 + \phi_2 + \phi_3$	0	0
SIN2	1	$f_1 + f_2 + f_3$	$U(0, 2\pi)$	0	0
SIN3	0.5	$f_1 + f_2 + f_3$	$U(0, 2\pi)$	0.5	$\phi_1 + \phi_2 + \phi_3$
SIN4	1	$f_1 + f_2 - f_3$	$\phi_1 + \phi_2 + \phi_3$	0	0
SIN5	1	$f_1 + f_2 - f_3$	$U(0, 2\pi)$	0	0

Test Case SIN1

In this case, the frequency of the fourth sinusoid is the sum of the frequencies of the other three sinusoids, and its phase is the sum of the phases of the other sinusoids.

$$f_4 = f_1 + f_2 + f_3 = 0.2668 \text{ Hz}$$

$$\phi_4 = \phi_1 + \phi_2 + \phi_3$$

This case therefore corresponds to four-wave interactions in which the fourth wave is forced by and phase-locked to the other three.

The T-tricoherence is a function of three independent frequency variables and so difficult to display. Here, we take slices through the axis of one frequency variable to show results in 2D, and we label the axes as f_1 , f_2 , and f_3 . Accordingly, an image of the T-tricoherence, for the slice $f_3 = f_1$; i.e. $T(f_1, f_2, f_3 = f_1)$, is given in Figure 1 on \log_{10} scale. The vertical and horizontal dashed lines correspond to the four frequencies, both in the same order as the vertical lines are labelled. The image is symmetric about the diagonal dashed line.

The dark blue corresponds to f_4 being outside the positive frequency range (top right region of the plot) or when the tricoherence value is less than 0.001. Considering the region for $f_1 < f_2$ (below the diagonal dashed line), the maximum (circled) tricoherence of 0.688 occurs at the triplet $f_1 = f_2$, $f_2 = f_3$, $f_3 = f_1$; i.e. the triplet (f_2, f_3, f_1) . The relatively large value of the tricoherence in this case reflects strong phase coupling at this combination of frequencies, as we might expect. Corresponding peaks at the other permutations of the f_1, f_2 , and f_3 triplet are also observed when similarly plotted.

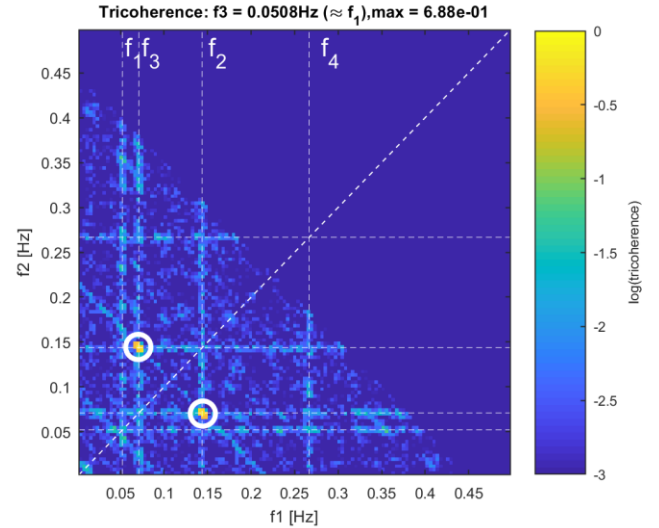


Figure 1 Image of T-tricoherence for $f_3 = 0.0508$ Hz for Case SIN1.

The corresponding V-tricoherence is given in Figure 2. The dark blue regions are as described for Figure 1. The maximum of 0.877 can be seen to occur at the triplet (f_1, f_1, f_1) , and the vertical and horizontal ridge of high values (at $f_1 = f_1$, $f_2 = f_1$) correspond to cases satisfying $f_1 + f_2 = f_3 + f_4$. The tricoherence is higher at values of f_1 and f_2 equal to any of the frequencies of the four sinusoids; these are referred to as trivial cases for the V-tricoherence.

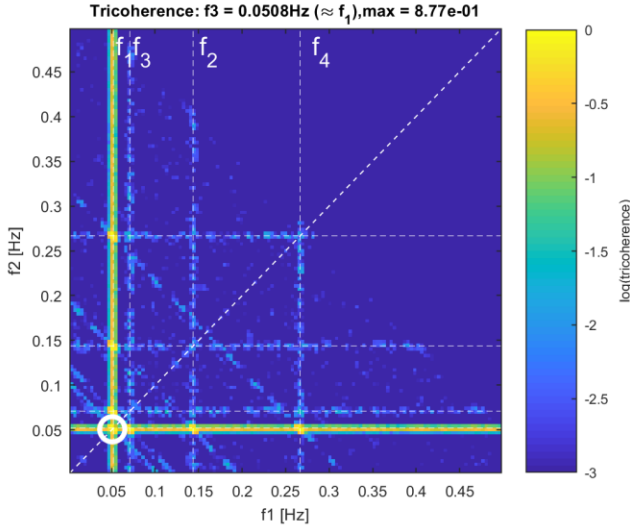


Figure 2 Image of V-tricoherence for $f_3 = 0.0508$ Hz for Case SIN1.

An overall picture of the tricoherence is achieved by computing the tricoherence maximum for a given value of f_3 (over all choices of f_1 and f_2) and plotting these maxima as a function of f_3 . Such f_3 maxima slices for both definitions of the tricoherence are plotted in Figure 3. Both show maxima at the frequencies f_1 , f_2 , and f_3 , but the V-tricoherence shows an additional peak at f_4 , which is not present in the T-tricoherence. The V-tricoherence also shows a higher background level of noise, probably associated with fortuitous matching of the condition $f_1 + f_2 = f_3 + f_4$.

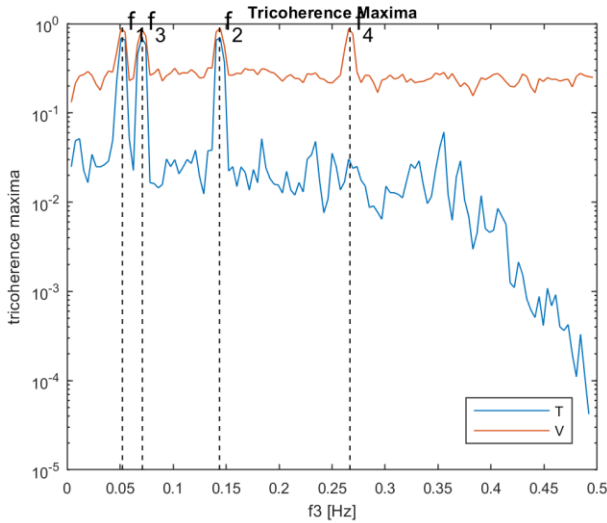


Figure 3 f_3 slice maxima for the T and V tricoherence estimates, for the phase-locked sinusoidal signal (SIN1).

Test Case SIN2

In this case, the signal is the same as for case SIN1, except that a random phase is assigned to the fourth sinusoid. This is achieved by selecting a different random phase for ϕ_4 at the

beginning of each segment. The phase for each segment is drawn from a uniform distribution over $[0, 2\pi)$.

The f_3 axis slice maxima for the two tricoherence definitions are given in Figure 4. The V-tricoherence is essentially unchanged (from Figure 3) by the introduction of the random phase. The T-tricoherence is however now absent of the peaks evident in the phase-locked case. Apparently, the V-tricoherence gives the same result, irrespective of whether or not the phases are locked or not. On the other hand, the T-tricoherence requires that the phases are locked to be detected above the noise floor.

Test Case SIN3

We also examined the effect of a partially phase-coupled fourth component by adding a fifth sinusoid, such that $f_5 = f_4$, $a_5 = 0.5$, $\phi_5 = \phi_1 + \phi_2 + \phi_3$, and setting $a_4 = 0.5$, effectively involving a fourth component split equally between a phase-coupled part and a random phase part. The f_3 axis slice maxima for the two tricoherence definitions are given in Figure 5. The V-tricoherence curve is unchanged from that in Figure 3. The T-tricoherence curve is similar that in Figure 3 – the level of the background noise is the same, but the peaks are reduced to about half the level of those in Figure 3. This confirms that partially-phase coupled components can be detected by the T-tricoherence and also that the amount of phase-coupling at a given combination of frequencies will be indicated.

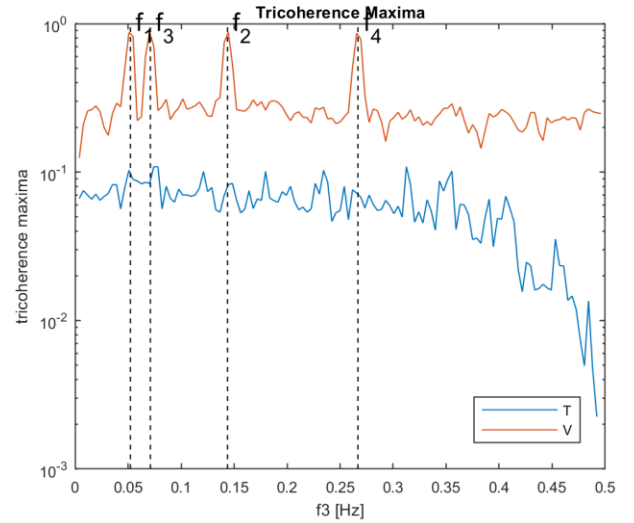


Figure 4 f_3 slice maxima for the T and V tricoherence estimates, for the sinusoidal signal for which the fourth component is assigned a random phase for each segment (Case SIN2).

Test Case SIN4

In this case, the signal is the same as for Case SIN1, except for the definition of f_4 . This case corresponds to the four-wave interaction $f_1 + f_2 = f_3 + f_4$. with locked phase.

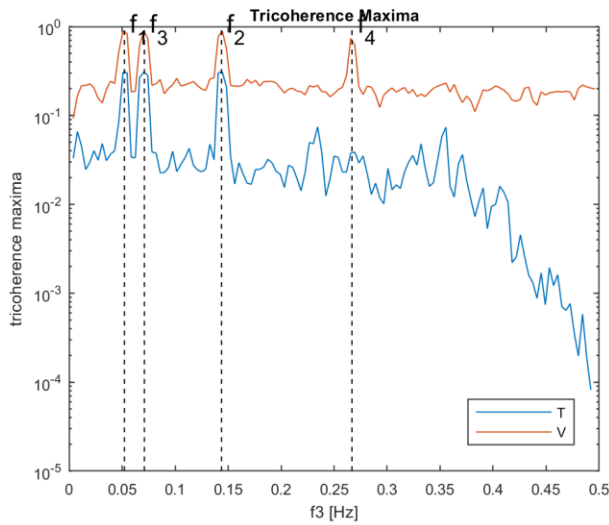


Figure 5 f_3 slice maxima for the T and V tricoherence estimates, for the partially phase-locked sinusoidal signal (Case SIN3).

The f_3 axis slice maxima for the two tricoherence definitions are given in Figure 6. Apart from a shift in the location of fourth sinusoid in the V-tricoherence, the spectra in Figure 6 are the same as those in Figure 4. However, as the combination of sinusoids do not satisfy the condition $f_4 = f_1 + f_2 + f_3$, none of the sinusoids is detected by the T-tricoherence definition.

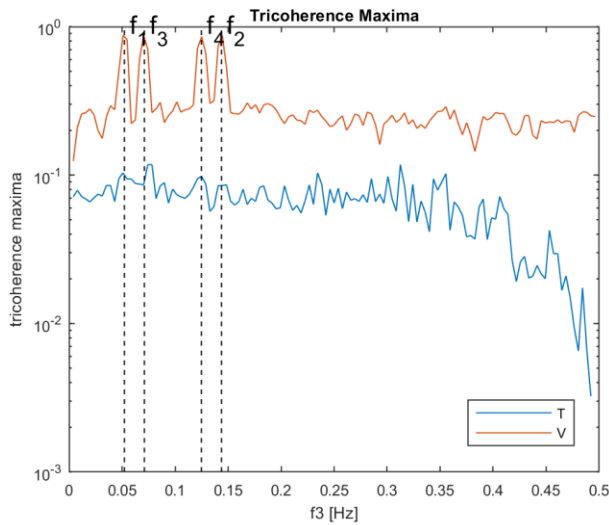


Figure 6 f_3 slice maxima for the T and V tricoherence estimates, for the sinusoidal signal of Case SIN4.

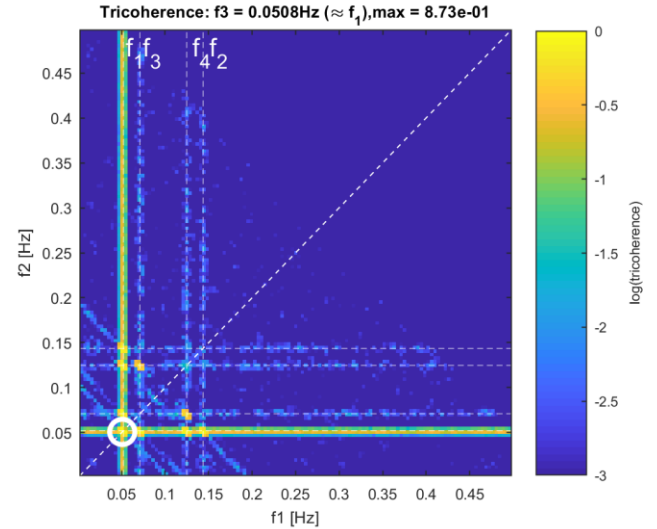


Figure 7 Image of V-tricoherence for $f_3 = 0.0508$ Hz for Case SIN4.

The image of the V-tricoherence, for the slice $f_3 = f_1$; i.e. $V(f_1, f_2, f_3 = f_1)$, is given in Figure 7. The high levels associated with the trivial cases of the same type as those identified in Figure 2 are seen Figure 7, but a significant peak can be noted for the Fourier frequencies 0.0508 Hz ($\approx f_1$), 0.0703 Hz ($\approx f_3$), and 0.125 Hz ($\approx f_4$), which is a triplet that satisfies the interaction condition for SIN4. This suggests that it is possible to identify four wave interactions of the SIN4 type with the V-tricoherence, when the frequencies of the four interacting components are different.

Test Case SIN5

In this case, the signal is the same as for Case SIN4, except that a random phase is assigned to the fourth sinusoid, as for Case 2. The results for this case are contrary to those for Case 3, showing that the V-tricoherence is sensitive to whether the phases of the components are phase-locked or not, for the case $f_1 + f_2 = f_3 + f_4$. The image of the V-tricoherence, for the slice $f_3 = f_1$; i.e. $V(f_1, f_2, f_3 = f_1)$, is given in Figure 8. By comparison with Figure 7, it is notable that the peak at the Fourier frequencies 0.0508 Hz ($\approx f_1$), 0.0703 Hz ($\approx f_3$), and 0.125 Hz ($\approx f_4$) is not present in Figure 8, indicating a lack of capability of the V-tricoherence to detect four wave interactions of SIN5 type – i.e. where one of the components has random phase.

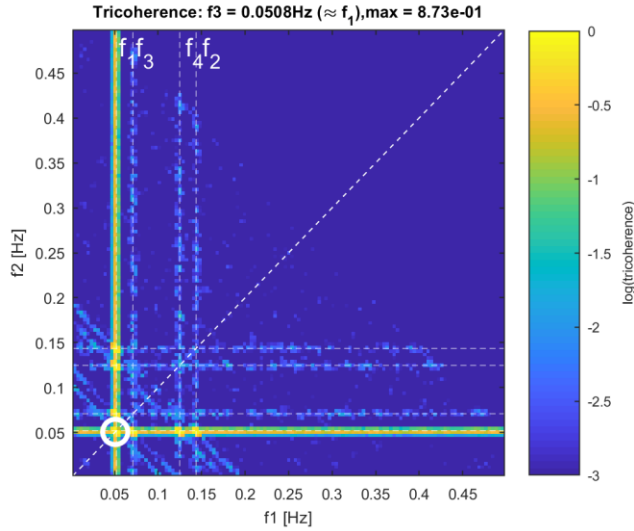


Figure 8 Image of V-tricoherence for $f_3 = 0.0508$ Hz for Case SIN5.

HOS MODEL SIGNAL

Numerical simulations were performed using the High-order Spectral (HOS) model that was developed in the LHEEA Laboratory at Ecole Centrale Nantes, France. HOS is a computationally-efficient, open-source model that can accurately simulate the nonlinear behaviour of surface waves propagating in the ocean (Ducrozet, *et al.*, 2012, Ducrozet, *et al.*, 2016). All simulations employed the HOS-ocean program to simulate unidirectional wave fields. The length of the computational domain L_x was set to $42\lambda_p$ (where λ_p is the wave length corresponding to the peak period T_p), the simulations were run for $235T_p$ with a Dommermuth initialisation of duration $10T_p$ and n equal to 4. The HOS order was set to 5, and 10^{-7} was used for tolerance of the Runge-Kutta Cash–Karp time marching scheme. HOS runs of order 3 would have been sufficient to produce the effects that the trispectrum is expected to identify, but real sea states are not limited to order 3, and we expect HOS model runs to order 5 might better indicate the performance of the trispectrum in a real sea state. Table 2 illustrates the unidirectional sea-state conditions that were simulated using the HOS model

Table 2: Key parameters for the HOS-ocean unidirectional simulations using the JONSWAP spectrum; H_s is the significant wave height, T_p is the peak period, γ is the peak enhancement factor, and d is the water depth.

Case	H_s [m]	T_p [s]	γ	d [m]
HOS1	5.0	16	2.5	Infinite
HOS2	10.0	16	2.5	Infinite
HOS3	12.5	16	2.5	Infinite
HOS4	15.0	16	2.5	Infinite
HOS5	15.0	16	2.5	65

HOS6	15.0	16	10.0	125
------	------	----	------	-----

The four simulations with infinite water depth progress from $H_s = 5$ m, through to $H_s = 15$ m, and so represent sea states of low to high steepness, in which the respective sea states are expected to be near linear to highly nonlinear. The finite depth simulations represent sea states that are expected to be highly nonlinear but being in shallow water ($k_p d \approx 1$ and 2 for the HOS5 and HOS6 cases respectively), a larger contribution of third-order bound terms are expected. We give focus in this paper to the analysis of the HOS4 and HOS5 records, which are expected to emphasise resonance and bound third-order interactions respectively.

The f_3 axis slice maxima for the two tricoherence definitions are given in Figure 9, for the HOS4 record. The plot shows high values of the V-tricoherence in the vicinity of the peak frequency, while the T-tricoherence does not show any significant values. This suggests that four wave interactions of the type $f_4 = f_1 + f_2 + f_3$ are not strong or not active, but those of the type $f_1 + f_2 = f_3 + f_4$ may be active - the latter point moderated in the light of our findings for the sine waves above and the fact that the maxima of the tricoherences were not found to be significantly different from those for the HOS1 record, which is expected to be substantially linear.

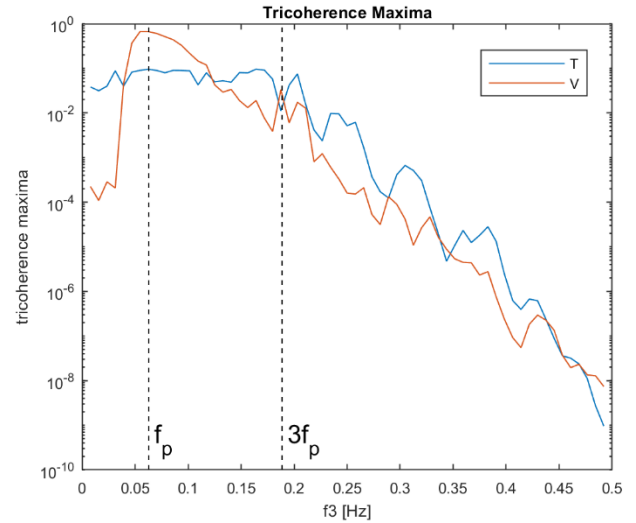


Figure 9 f_3 slice maxima for the T and V tricoherence estimates, for the HOS4 signal (Table 2).

The trispectrum slices for $f_3 = f_p$ for the T- and V-tricoherence estimates are given in Figure 10 and Figure 11 respectively - f_p is the peak frequency of the power spectrum and is the frequency about which the V-tricoherence attains its largest values. The T-tricoherence has increased levels around f_p , but they are low (<0.1) and diffused over a relatively broad frequency range. In contrast to this, the V-tricoherence (Figure

11) has significant values around f_p and is sharply focussed about f_p .

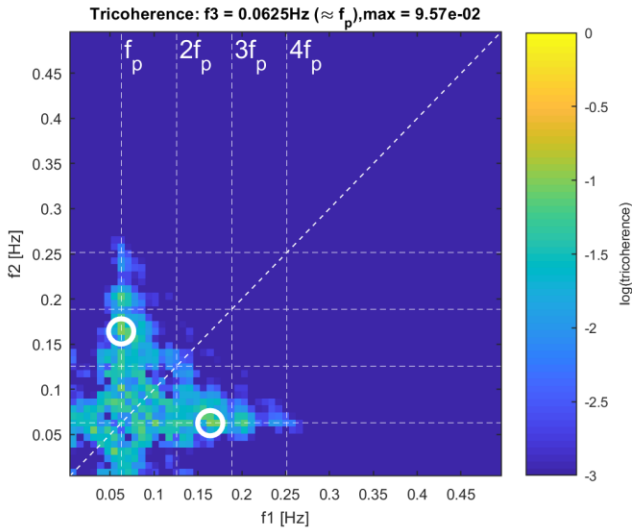


Figure 10 T-tricoherence slice at $f_3 = f_p$ for the HOS4 signal

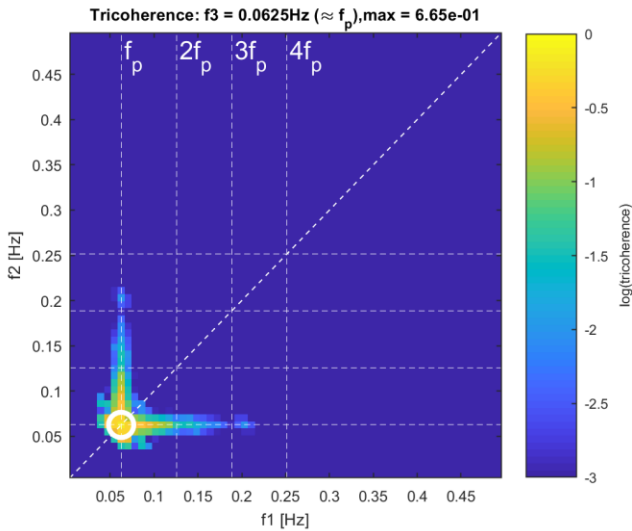


Figure 11 V-tricoherence slice at $f_3 = f_p$ for the HOS4 signal.

The f_3 axis slice maxima for the two tricoherence definitions for the HOS5 record are given in Figure 12. The tricoherence curves are very similar to those for the HOS4 signal (Figure 9), but with indications of slightly higher T-tricoherence values at low frequency (≈ 0.025 Hz), perhaps reflecting the presence of third-order difference frequency effects.

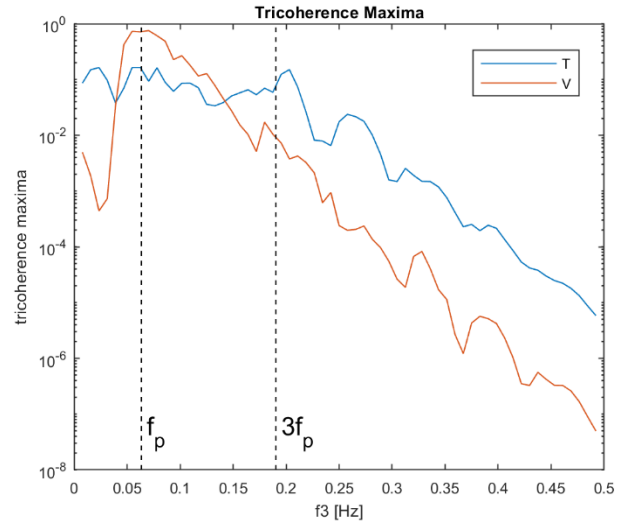


Figure 12 f_3 slice maxima for the T and V tricoherence estimates, for the HOS5 signal (Table 2).

LABORATORY DATA

The laboratory record considered here was taken from experiments carried out at the MARINTEK Ocean Basin in Trondheim, Norway. The Basin has a water surface area of 50 m by 70 m with a variable depth of up to 10 m. The Basin is capable of producing multi-directional waves up to 0.4 m high at periods above 0.6 s. The particular record presented here is a combination of two irregular waves one with a peak enhancement parameter of 6 and the other 3. The combined significant wave height is 0.058 m, and the peak period of both irregular waves is 1 s. The water depth was 3 m.

The f_3 axis slice maxima for the two tricoherence definitions are given in Figure 13. These curves are similar to those for the HOS spectra, with similar peak values, suggesting similar interpretation – i.e. possibly four wave interactions of the type where $f_1 + f_2 = f_3 + f_4$, but not of the type $f_4 = f_1 + f_2 + f_3$ that are phase-locked. The peak in the V-tricoherence at approximately $3f_p$ is notable, but with a peak value of around 0.01, it must be considered insignificant.

The f_3 axis slice images are similar to those for the HOS spectra; that for the V-tricoherence at $f_3 \approx f_p$ is given in Figure 14, for example.

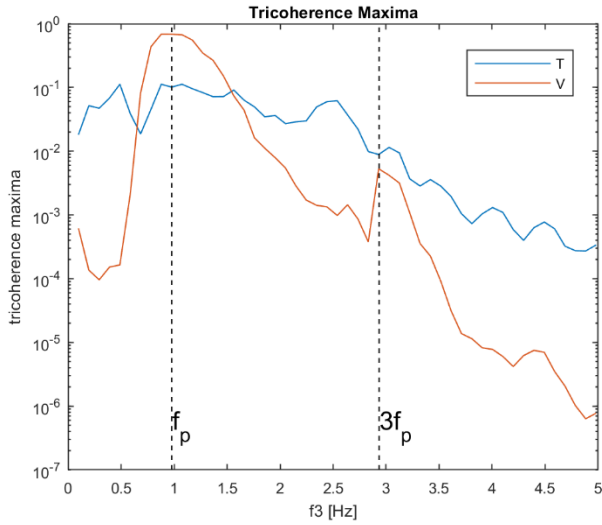


Figure 13 f_3 slice maxima for the T and V tricoherence estimates, for the laboratory signal.

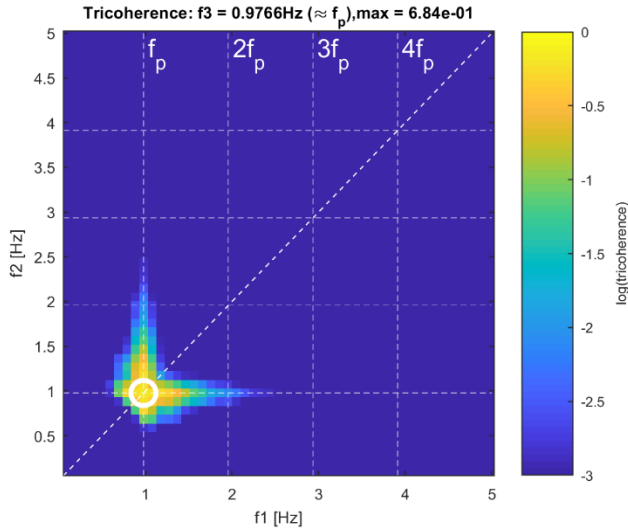


Figure 14 V-tricoherence slice at $f_3 = f_p$ for the laboratory signal.

DRAUPNER WAVE RECORD

The final record that we consider is a field measurement recorded at the Draupner platform on 1 January 1995. This record includes the unusually high crest event (Haver and Andersen, 2000) that has received much attention. The Draupner location is in the North Sea where the water depth is 70 m. The wave measurements were made with a laser wave sensor.

The f_3 axis slice maxima for the two tricoherence definitions are given in Figure 15. These curves are similar to those for the HOS and laboratory spectra, with similar peak values, although the maximum T-tricoherence value is approximately twice those of the HOS and laboratory maxima but still remains effectively insignificant. Thus, a similar interpretation begs – i.e. there is evidence of four wave

interactions of the type where $f_1 + f_2 = f_3 + f_4$, but not of the type $f_4 = f_1 + f_2 + f_3$ that are phase-locked.

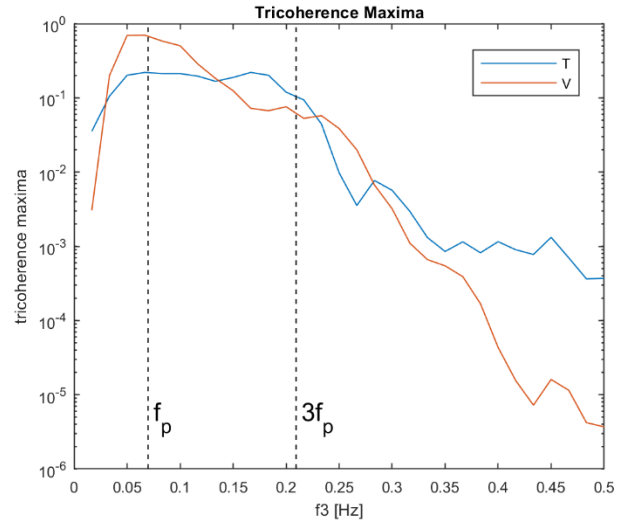


Figure 15 f_3 slice maxima for the T and V tricoherence estimates, for the Draupner wave record signal.

Although not materially different from the HOS and laboratory examples, we provide f_3 axis slice images for the T-tricoherence in Figure 16 and V-tricoherence in Figure 17 for $f_3 \approx f_p$ on account of the historical interest in the Draupner wave record and because we believe this is the first example of trispectral analysis of this record to be published. The images in these two figures have a lower resolution than the earlier examples, due to the lower sampling frequency of the Draupner measurements and our objective to reduce sampling variability in the estimates as far as practical. The images in Figure 16 and Figure 17 are qualitatively similar to the earlier examples, when consideration is given to the different resolutions involved.

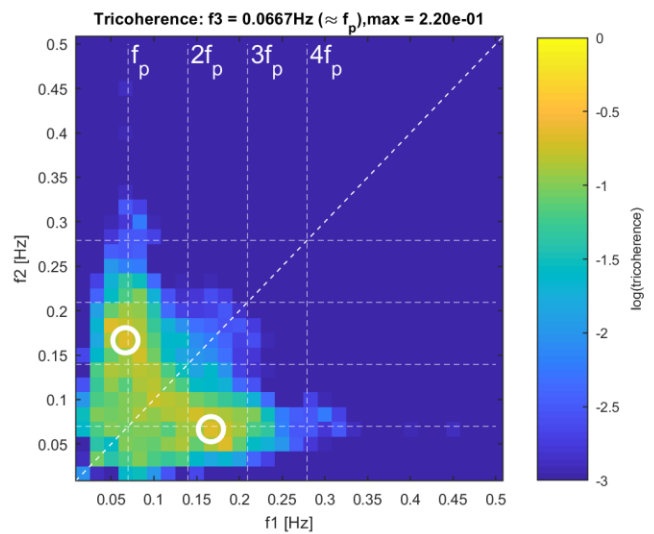


Figure 16 T-tricoherence slice at $f_3 = f_p$ for the Draupner wave record signal.

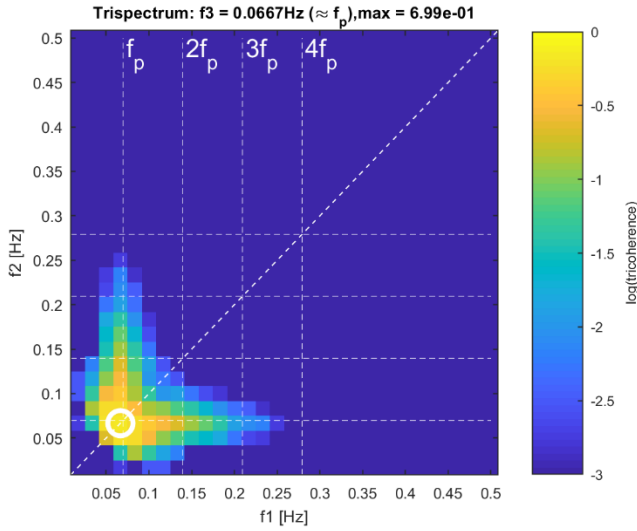


Figure 17 V-tricoherence slice at $f_3 = f_p$ for the Draupner wave record signal.

DISCUSSION

Bispectra and trispectra provide representations of higher-order effects in sea states, in the Fourier sense. That is, analysis and interpretation is based on the record duration of the Fourier transform. Thus, short-term effects, such as localised nonlinear effects, are effectively averaged together with the rest of the record, which may be mostly linear. Accordingly, important highly nonlinear events will be watered down and may even be missed. Attempts to overcome this, at least in the case of bispectral analysis, by incorporating the analysis in wavelet analyses have been shown to have some success in identifying nonlinear events in water wave records (Ewans and Buchner, 2008, Dong *et al.*, 2008) and in other phenomena (van Milligen *et al.*, 1995, Larsen and Hanssen, 2000, and Schulte, 2016,). It remains to be seen whether a wavelet approach can be extended to the incorporation of trispectra in wavelet analysis, to produce additional insight.

It might be expected that trispectra are limited to identifying only the class of four-wave interactions that are phase locked (see Appendix), thus providing no information on resonant interactions. However, the analysis reported here indicates that the application of both the T- and V-trispectral analyses may allow the possibility to assess whether or not four-wave interactions are phase-locked or not. This remains to be substantiated. For example, the Zakharov equation provides a Hamiltonian formulation for the evolution of the surface elevation. Using this formulation, it is possible to determine contributions at various orders of nonlinearity and from different sources, i.e. bound and resonant wave-wave interactions; this should provide an ideal testbed for trispectral analysis methods.

By definition, the V-tricoherence will indicate large values whenever the condition $f_1 + f_2 = f_3 + f_4$ is satisfied. For example, high values of V-tricoherence will occur when $f_1 = f_3$ and $f_2 = f_4$ (or $f_1 = f_4$ and $f_2 = f_3$) irrespective of whether four wave interactions are active or not; the case when $f_1 = f_2 = f_3 =$

$f_4 = f_p$ is a particularly relevant case in point, given the high V-tricoherence values we observed in the vicinity of the peak frequency in our results. The “trivial” solutions result from interactions between two pairs of components but not necessarily all four components together. Apparently, the trivial solutions correspond to events where interactions between components can be divided into groups that are statistically independent of each other and can be avoided by considering the cumulant based trispectrum rather than the moment-based trispectrum (Kravtchenko-Berejnoi *et al.*, 1995). Molle and Hinich (1995) provide a good description of the difference between cumulant-based and moment-based trispectra. It is clear from the definition of the trispectrum that it strongly depends on the amplitudes of the Fourier components involved. Kravtchenko-Berejnoi *et al.* (1995) suggest using the normalisation of Brillinger (1965) to obtain explicit information about the contribution of wave-wave interaction to the power of a certain oscillation. We are currently investigating the Kravtchenko-Berejnoi *et al.* (1995) approach, and preliminary results of f_3 slice maxima applied to the HOS5 record (Table 2) and to the Draupner record are given in Figure 18 and Figure 19 respectively. The f_3 slice maxima corresponding to the Kravtchenko-Berejnoi *et al.* (1995) tricoherence definition is the yellow line (K) line in each plot, while those for the T- and V-tricoherences are the same as in Figure 12 and Figure 15. The plots show reduced K-tricoherence levels by comparison with the V-tricoherence levels in the vicinity of the spectral peak, substantially so in the case of the Draupner records, perhaps indicating removal of the contribution from the “trivial” solutions. The plots also show increased K-tricoherence levels by comparison with the V-tricoherence levels in the region around $3f_p$, and also at higher frequencies in the case of the Draupner records.

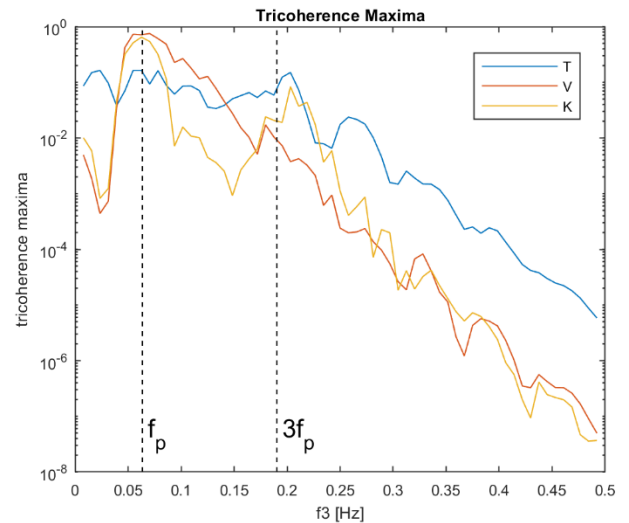


Figure 18 f_3 slice maxima for the T and V tricoherence estimates, for the HOS5 signal (Table 2), as in Figure 12, plus those using the Kravtchenko-Berejnoi *et al.* (1995) tricoherence definition (K).

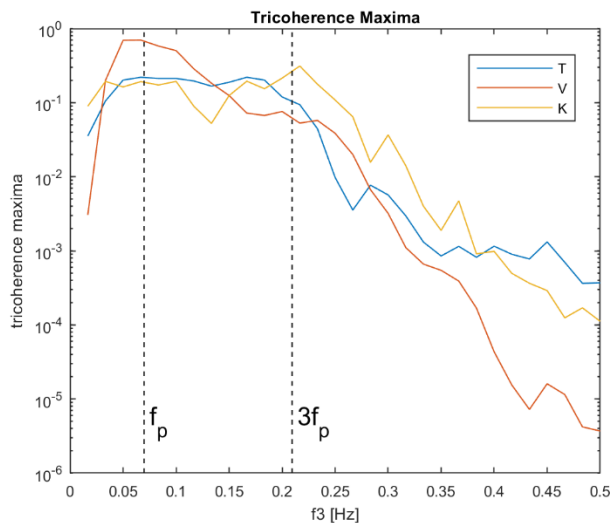


Figure 19 f_3 slice maxima for the T and V tricoherence estimates, for the Draupner signal, as in Figure 15, plus those using the Kravtchenko-Berejnoi *et al.* (1995) tricoherence definition (K).

We have yet to incorporate uncertainty statistics, such as bias and variance, of our estimates; but these are well documented in the literature (e.g. Chandran *et al.* 1994) and it is our intention to include these in the form of error bars or noise floor levels, as appropriate in the various graphical presentations. Similarly, we intend to improve the clarity of our frequency-slice images by removing the redundant subdomains of the tricoherence functions, such as the region where $f_2 > f_1$.

Finally, we note the application of the nonlinear Fourier analysis (NLFA) method (Osborne 2010), which provides (perhaps a superior) alternative to higher-order spectra that are based on conventional Fourier analysis, to investigate nonlinear effects in data sets. An example of the application of the NLFA on wave data is given by Osborne *et al.* (2018). Osborne *et al.* (2018) remark that distinguishing characteristic of the NLFA method is its ability to spectrally decompose a time series into its nonlinear coherent structures (Stokes waves and breathers) rather than just sine waves. This is done by the implementation of multidimensional, quasiperiodic Fourier series, rather than ordinary Fourier series.

CONCLUSIONS

The T-tricoherence provides the capability to detect phase-locked four wave interactions of the form $f_4 = f_1 + f_2 + f_3$, that is where three waves interact to force a bound fourth component. However, our estimates of the T-tricoherence on nonlinear wave simulations, and measured laboratory and field (Draupner) records did not indicate significant four wave interactions of this type. While this result is expected for deep-water cases, we might have expected larger T-tricoherence values for the HOS5 (Table 2) case, for which $k_p d \approx 1$.

Estimates of V-tricoherence produce high values at frequency triplets that correspond to high Fourier amplitudes. It

is not possible to conclude whether these indicate the occurrence of actual four wave interactions of the type $f_1 + f_2 = f_3 + f_4$, or whether they simply indicate combinations of independent pairs of Fourier components that happen to satisfy the frequency relationship. It is likely though that these four-wave interactions are present, in some of the sea states we investigated. We are currently investigating alternative tricoherence estimators to differentiate between these two possibilities or to exclude contributions from trivial combinations in the moment estimates.

REFERENCES

- Aubourg, Q., Campagne, A., Peureux, C., Ardhuin, F., Sommeria, J., Viboud, S., and N. Mordant (2017). Three-wave and four-wave interactions in gravity wave turbulence. *Phys. Rev. Fluids*, 2, 114802-1 – 114802-19.
- Barber, N.F., and F. Ursell (1948). The generation and propagation of ocean waves and swell. *Phil. Trans. Roy. Soc.* bfA240, 527-560.
- Brillinger, D. (1965). An introduction to polyspectra. *Annals of Mathematical Statistics*, 36, 1351–1374.
- Chandran, V., Elgar, S., and B. Vanhoff (1994). Statistics of tricoherence. *IEEE Trans. Sig. Proc.*, 42, 12, pp 3430-3440.
- Cherneva, Z., and C. Guedes Soares (2007). Estimation of the bispectra and phase distribution of storm sea states with abnormal waves. *Ocean Engineering*, 34, pp 2009-2010.
- Dalle Molle, J.W., and M.J. Hinich (1995). Trispectral analysis of stationary random time series. *Journal of the Acoustical Society of America*, 97, 2963-2978.
- Dong, G., Ma, Y., Perlin, M., Ma, X., Yu, B., and J. Xu (2008). Experimental study of wave-wave nonlinear interactions using the wavelet-based bicoherence. *Coastal Engineering*, 55, pp 741-752.
- Ducrozet, G., Bingham, H.B., Engsig-Karup, A.P., Bonnefoy F., and P. Ferrant (2012) A comparative study of two fast nonlinear free-surface water wave models, *International Journal of Numerical Methods in Engineering*, volume 69, number 11, pages 1818–1834.
- Ducrozet, G., Bonnefoy, F., Le Touz , D., and P. Ferrant (2016) HOS-ocean: Open-source solver for nonlinear waves in open ocean based on High-Order Spectral method, *Computer Physics Communications*, volume 203, pages 245–254.
- Elgar, S., and R.T., Guza (1985). Observations of bispectra of shoaling surface gravity waves. *Journal of Fluid Mechanics* 161, 425–448.
- Elgar, S., Herbers, T.H.C., Chandran, V., and R.T. Guza (1995). Higher-order spectral analysis of nonlinear ocean surface gravity waves. *J. Geophys. Res.*, 100, C3, pp 4977-4983.
- Ewans, K.C., and Buchner, B. (2008). Wavelet analysis of an extreme wave in a model basin. *Proceedings of 27th International Conference on Offshore Mechanics and Arctic Engineering*, 15-19 June 2008, Estoril, Portugal
- Harris, F. J., 1978. On the use of windows for harmonic analysis with the discrete Fourier transform. *Proceedings of the IEEE*, 66, No. 1, pp 51-83.

Hasselmann, K., Munk, W., and G., Mc Donald (1963). Bispectra of ocean waves. In: Rosenblatt, M. (Ed.), *Time Series Analysis*. Wiley, NY, pp.125–139.

Haubrich, R.A. (1965). Earth noise, 5 to 500 millicycles per second 1. *J. Geophys. Res.*, pp 1415-1427.

Haver, S. and Andersen, O. J., 2000: “ Freak waves – Rare Realizations of a Typical Population or Typical Realizations of a Rare Population?”, *Proceedings of ISOPE '2000*, June 2000, Seattle.

Kim, Y.C., and E.J. Powers (1979). Digital bispectral analysis and its applications to nonlinear wave interactions. *IEEE Trans. Plasma Sci.*, PS-7, 2, pp 120-131.

Kravtchenko-Berejnoi, V., Lefevre, F., Krasnosel'skikh, V., and D. Laoutte (1995). On the use of tricoherent analysis to detect non-linear wave-wave interactions. *Signal Processing*, 42, pp 291-309.

Larsen, Y., and A. Hanssen (2000). Wavelet-polyspectra: analysis of non-stationary and non-gaussian/non-linear signals. *Proceedings of the Tenth IEEE Workshop on Statistical Signal and Array Processing*, August 14- 16, Pocono Manor, USA.

Osborne, A.R. (2010). Nonlinear ocean waves and the inverse scattering transform. *Academic Press*, Boston.

Osborne, A.R., Resio, D., Costa, A., Ponce de Leon, S., and E. Chirivi (2018). Highly nonlinear wind waves in Currituck Sound: dense breather turbulence in random ocean waves. *Ocean Dynamics*, <https://doi.org/10.1007/s10236-018-1232-y>.

Pierson, W.J., and W. Marks (1952). The power spectrum analysis of ocean wave record. *Trans. Amer. Geophys. Un.* 33, 834-844.

Schulte, J.A. (2016). Wavelet analysis for non-stationary, nonlinear time series. *Nonlin. Processes Geophys*, 23, pp 257-267.

Toffoli, A., Onorato, M., Babanin, A.V., Bitner-Gregersen, E., Osborne, A.R., and J. Monbaliu, 2007. Second-order theory and set-up in surface gravity waves: a comparison with experimental data. *J. Phys. Ocean.*, 37(11), pp 2726–2739.

Tukey, J.W. (1949). The sampling theory of power spectrum estimates. *Symposium on Applications of Autocorrelation Analysis to Physical Problems, NAVEXOS-0-735*. Office of Naval Research.

Van Milligen, B.P., Sanchez, E., Estrada, T., Hidalgo, C., and B. Branas. Wavelet bicoherence: A new turbulence analysis tool. *Phys. Plasmas*, 2, pp 3017-3032.

Welch, P. D., 1967. The use of fast Fourier transform for the estimation of power spectra: a method based on time averaging over short, modified periodograms. *IEE Transactions on Audio and Electroacoustics*, AU-15, 2, pp 70-73.

APPENDIX

Introduction

Consider a time-series $x(t) = \sum_{j=1}^4 \cos(\omega_j^0 t + \phi_j^0)$, for $t \in (-\infty, \infty)$, for real angular frequencies $\{\omega_j^0\}$ and phases $\{\phi_j^0\}$. The Fourier transform of $\exp(i\omega_j^0 t)$ is given by $2\pi\delta(\omega - \omega_j^0)$ for $\omega \in (-\infty, \infty)$. Then it is straightforward to calculate the Fourier transform of $x(t)$ to be

$$\begin{aligned} X(\omega) &= \sum_{j=1}^4 \int_{-\infty}^{\infty} \cos(\omega_j^0 t + \phi_j^0) e^{-i\omega t} dt \\ &= \pi \sum_{j=1}^4 e^{i\phi_j^0} \delta(\omega - \omega_j^0) + e^{-i\phi_j^0} \delta(\omega + \omega_j^0). \end{aligned}$$

Using this result, it is relatively straightforward to calculate the values of different trispectral estimators in closed form. It is also possible to calculate the statistical properties of trispectrum and tricoherence estimators for more general Gaussian series (with random Gaussian coefficients), as discussed in the full paper accompanying this work. Here we restrict attention to the simplest useful cases to motivate thinking as clearly as possible.

T-trispectrum

For arbitrary angular frequencies $\{\omega_j\}$, we assume that $T(\omega_1, \omega_2, \omega_3) = X(\omega_1)X(\omega_2)X(\omega_3)X^*(\omega_1 + \omega_2 + \omega_3)$. Now we set $\omega_4^0 = \omega_1^0 + \omega_2^0 + \omega_3^0$ for our time-series simulation above. We then see that

$$T(\omega_1^0, \omega_2^0, \omega_3^0) = \pi^4 e^{i(\phi_1^0 + \phi_2^0 + \phi_3^0 - \phi_4^0)}.$$

Fixed phases: For fixed values of $\{\phi_j^0\}$, it is obvious that the value of $T(\omega_1^0, \omega_2^0, \omega_3^0)$ will be non-zero and complex. In particular, $T(\omega_1^0, \omega_2^0, \omega_3^0)$ will be real only when $\phi_1 + \phi_2 + \phi_3 - \phi_4 = 2\pi n$, for $n = 0, \pm 1, \pm 2, \dots$. That is, when phases are coupled as specified, the trispectrum is real.

Multiple realisations with random phases: If we assume that each ϕ_j is uniformly distributed on $[0, 2\pi)$, and that we have n occurrences $\{x_k(t)\}$ of $x(t)$ corresponding to different random draws of the phases, and corresponding estimates $\{T_k(\omega_1^0, \omega_2^0, \omega_3^0)\}$, then since $\int_0^{2\pi} e^{i\phi} d\phi = 0$, we will have $E[T(\omega_1^0, \omega_2^0, \omega_3^0)] = \left(\frac{1}{n}\right) \sum_k T_k(\omega_1^0, \omega_2^0, \omega_3^0) = 0$. That is, for multiple intervals of time-series with random phases, the expected trispectrum is zero. Note however if we take the **absolute values** of trispectra, that $E[|T(\omega_1^0, \omega_2^0, \omega_3^0)|] = \left(\frac{1}{n}\right) \sum_k |T_k(\omega_1^0, \omega_2^0, \omega_3^0)| = \pi^4$.

V-trispectrum

Suppose now that we assume that $V(\omega_1, \omega_2, \omega_3) = X(\omega_1)X(\omega_2)X^*(\omega_3)X^*(\omega_1 + \omega_2 - \omega_3)$, and that we set $\omega_4^0 = \omega_1^0 + \omega_2^0 - \omega_3^0$ in the original time-series simulation, corresponding to the expected ocean wave 4-wave interaction. With this setting, we see that

$$V(\omega_1^0, \omega_2^0, \omega_3^0) = \pi^4 e^{i(\phi_1^0 + \phi_2^0 - \phi_3^0 - \phi_4^0)}.$$

In this situation, for fixed phases $\{\phi_j^0\}$, $V(\omega_1^0, \omega_2^0, \omega_3^0)$ will be complex unless $\phi_1^0 + \phi_2^0 - \phi_3^0 - \phi_4^0 = 2\pi n$, for $n = 0, \pm 1, \pm 2, \dots$ for which $V(\omega_1^0, \omega_2^0, \omega_3^0) = \pi^4$. For multiple realisations of time-series with random phases, the expected value $E[V(\omega_1^0, \omega_2^0, \omega_3^0)] = 0$; but again, as for the T-trispectrum, we note the effect of taking absolute values.

In the Section entitled “Tricoherence of sinusoids” in the main text, we consider time-series of the form $y(t) = x(t) + \alpha(t)$ where $\alpha(t)$ is additive Gaussian (white) noise. The Fourier transform of $\alpha(t)$ is a constant at all frequencies by definition: $A(\omega) = \kappa$. This means that numerous trivial combinations of frequencies will always yield non-zero values of V-trispectrum. For instance, for $j = 1, 2, 3, 4$ and any ω_2

$$V(\omega_j^0, \omega_2, \omega_j^0) = |(X + A)(\omega_j^0)|^2 |(X + A)(\omega_2)|^2 \approx \pi^2 \kappa^2$$

if $\pi \gg \kappa > 0$. This occurs regardless of phase specifications (since phase relationships are also trivially satisfied in such cases). These trivial combinations do not occur for the T-trispectrum.